Supporting Information

Highly thermal-stable white-emitting $Ca_9ZnK(PO_4)_7:Ce^{3+},Dy^{3+}$ single-phase phosphor: Tunable photoluminescence and energy transfer

Youkui Zheng,[a] Zizheng Wang,[a] Dan Yang,[a] Zhenyu Fang,[a] Yuefei Xiang,[a] Tongsheng Yang,[a] Shuqing Yang,[a] Yong Mao,[b] Kai Xiong*[b] and Jing Zhu*[a]

[a]*Yunnan Key Laboratory for Micro/nano Materials & Technology, Key Laboratory of LCR Materials and Devices of Yunnan Province, School of Materials and Energy, Yunnan University, Kunming 650091, China.*

[b]*Materials Genome Institute, Yunnan University, Kunming 650091, China.*

**Corresponding author.*

E-mail address: jzhu@ynu.edu.cn and xiongkai@ynu.edu.cn

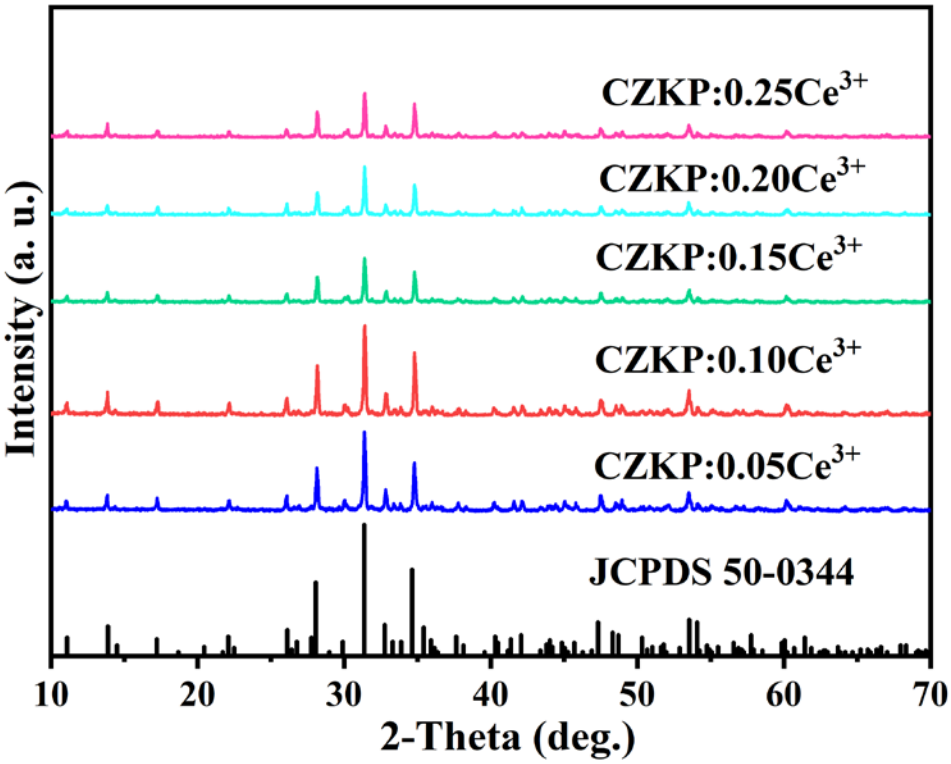

Fig. S1 PXRD patterns of Ce^{3+}-doped CZKP.

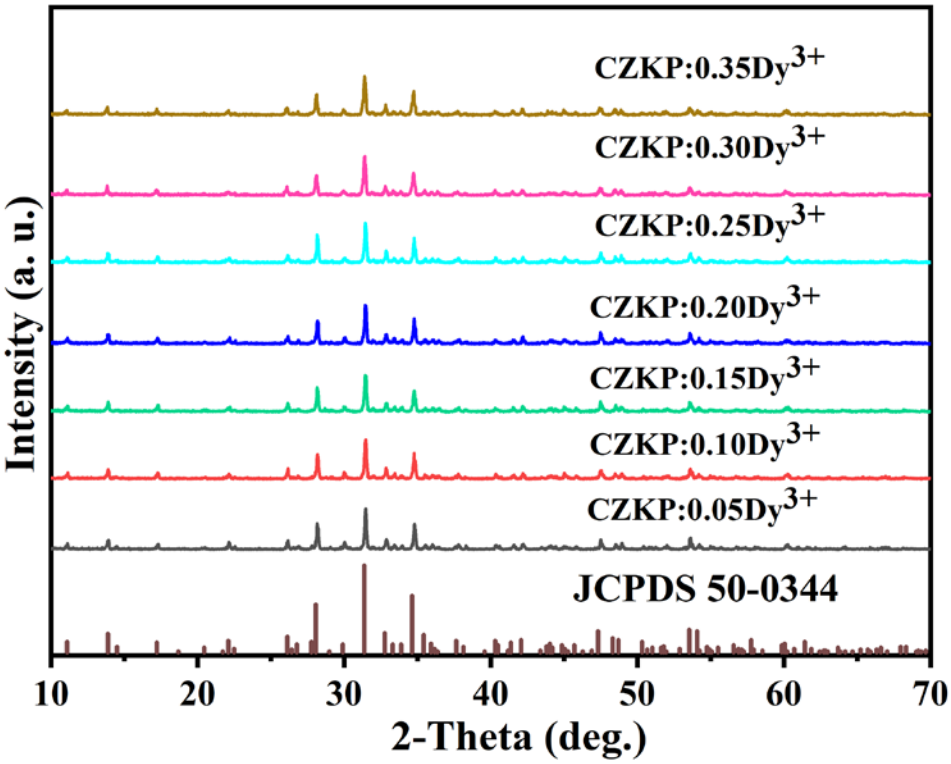

Fig. S2 PXRD patterns of Dy^{3+}-doped CZKP.

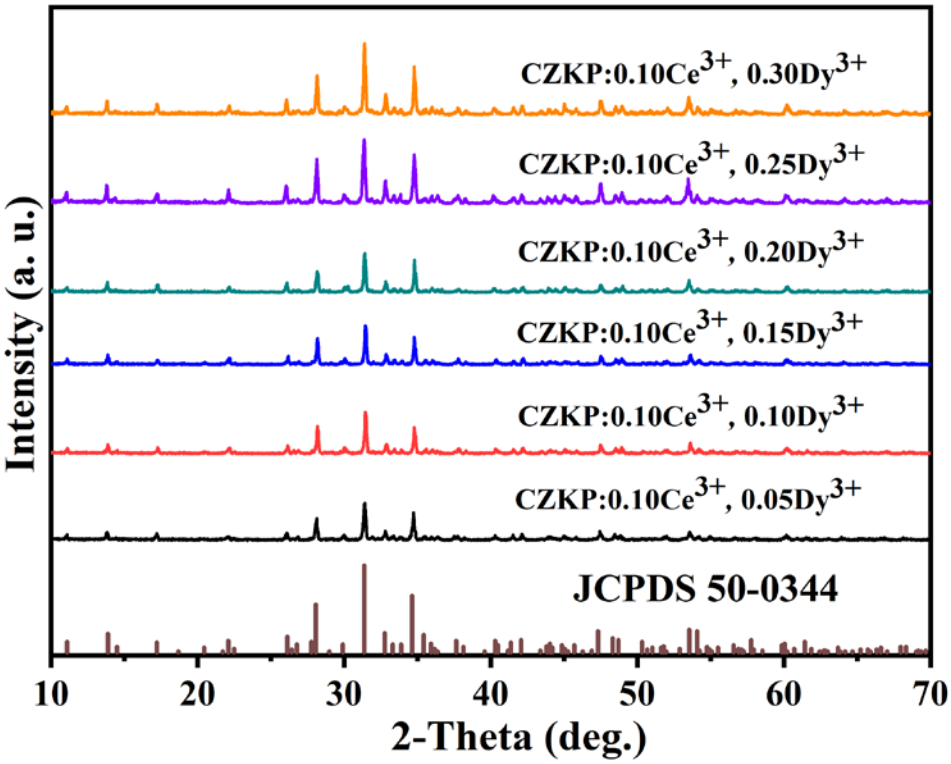

Fig. S3 PXRD patterns of Ce^{3+},Dy^{3+}-codoped CZKP.

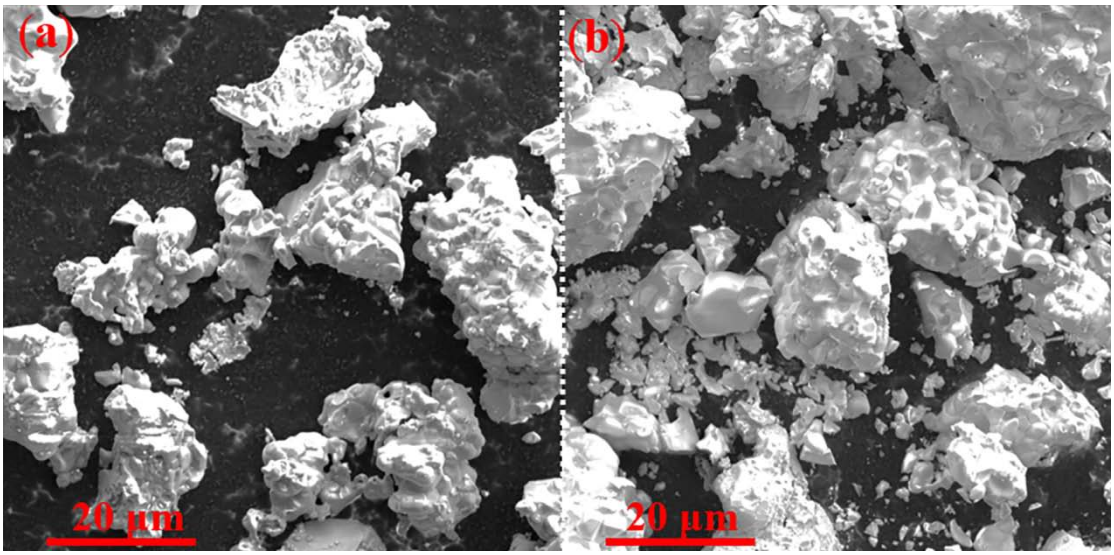

Fig. S4 (a) FESEM image of CZKP. (b) FESEM image of CZKP:0.10Ce^{3+},0.15Dy^{3+}.

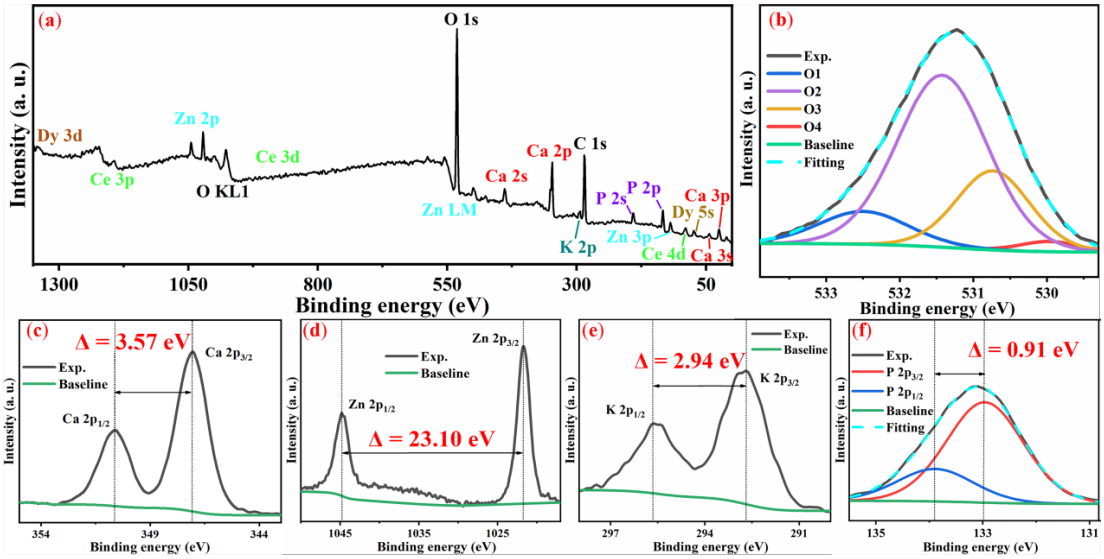

Fig. S5 XPS spectra of (a) survey, (b) O 1s, (c) Ca 2p, (d) Zn 2p, (e) K 2p, and (f) P 2p for CZKP:0.10Ce^{3+},0.15Dy^{3+}.

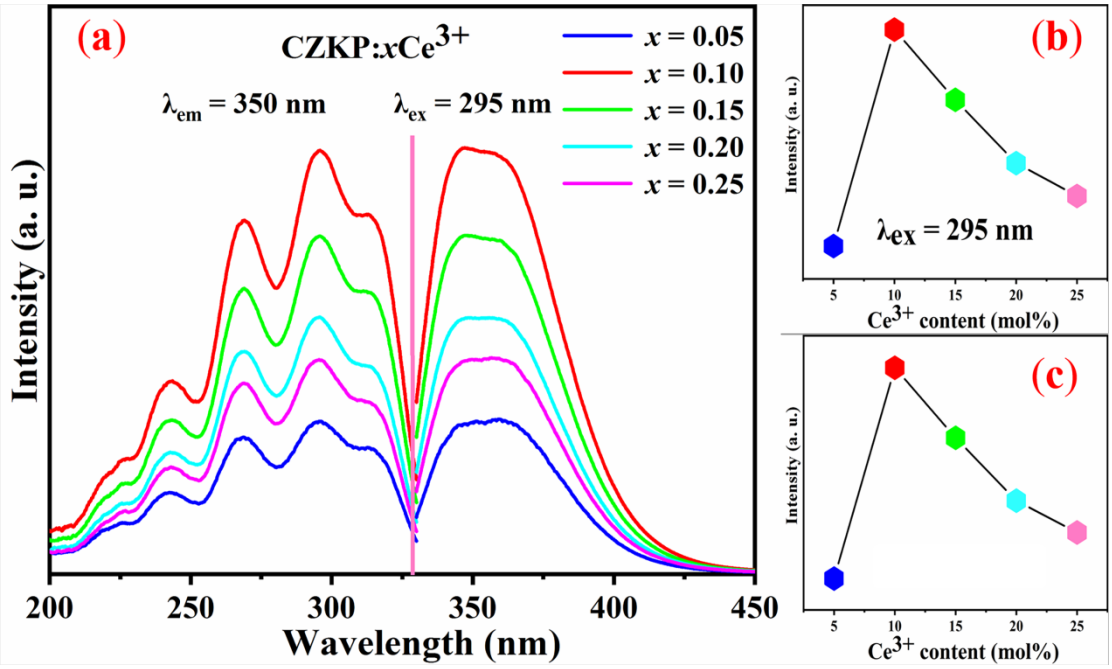

Fig. S6 (a) PLE and PL spectra of the CZKP:Ce^{3+} samples. (b) Influence of Ce^{3+} content on 295 nm excitation intensity. (c) Influence of Ce^{3+} content on integral emission intensity.

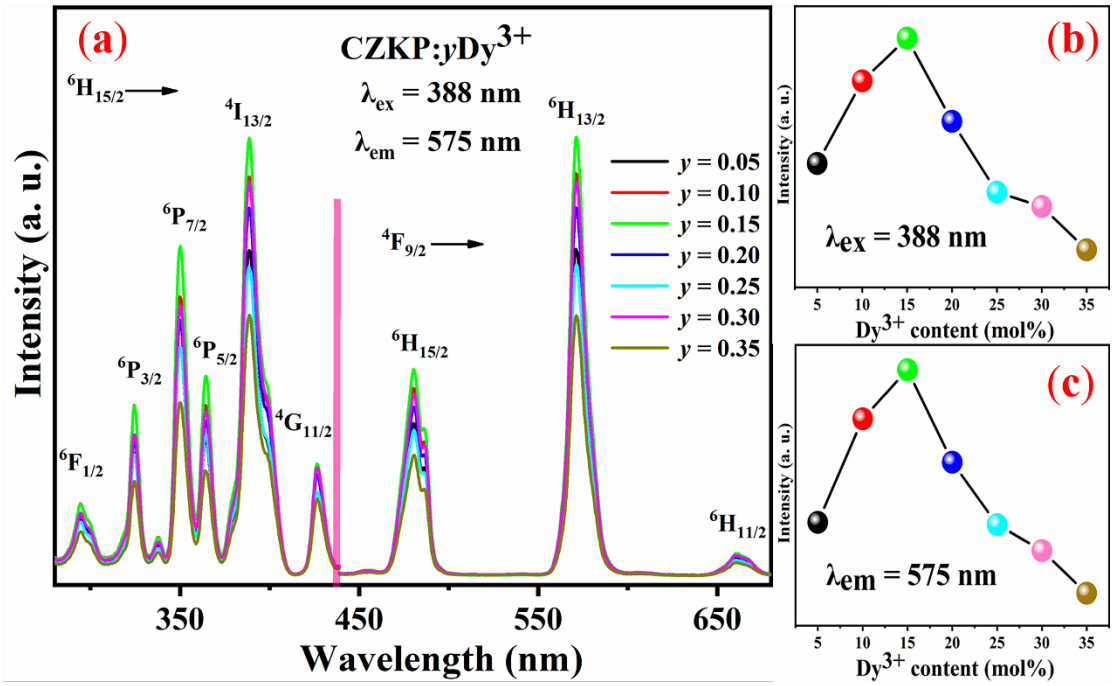

Fig. S7 (a) PLE and PL spectra of the CZKP:Dy^{3+} samples. (b) Influence of Dy^{3+} content on 388 nm excitation intensity. (c) Influence of Dy^{3+} content on integral emission intensity.

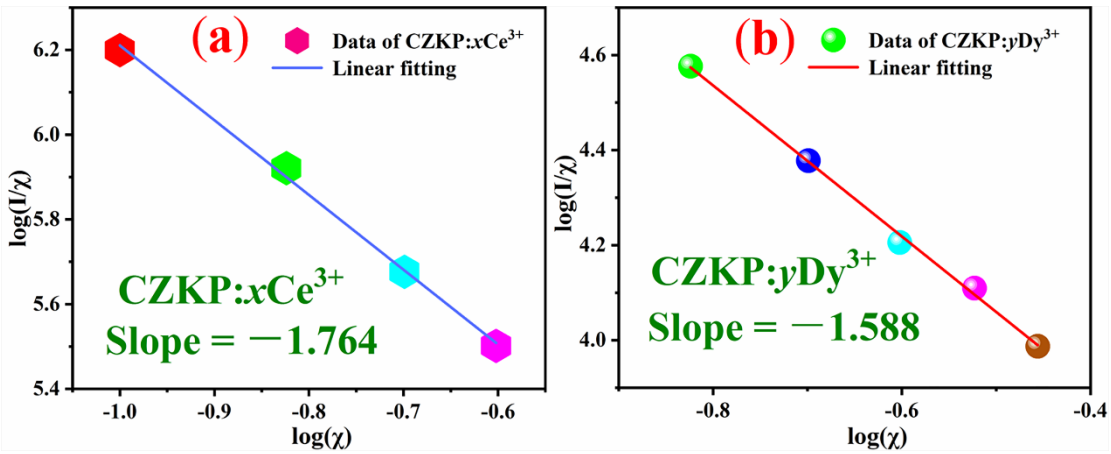

Fig. S8 Plot of log(I/χ) as function of log(χ) in (a) CZKP:xCe^{3+} and (b) CZKP:yDy^{3+}.

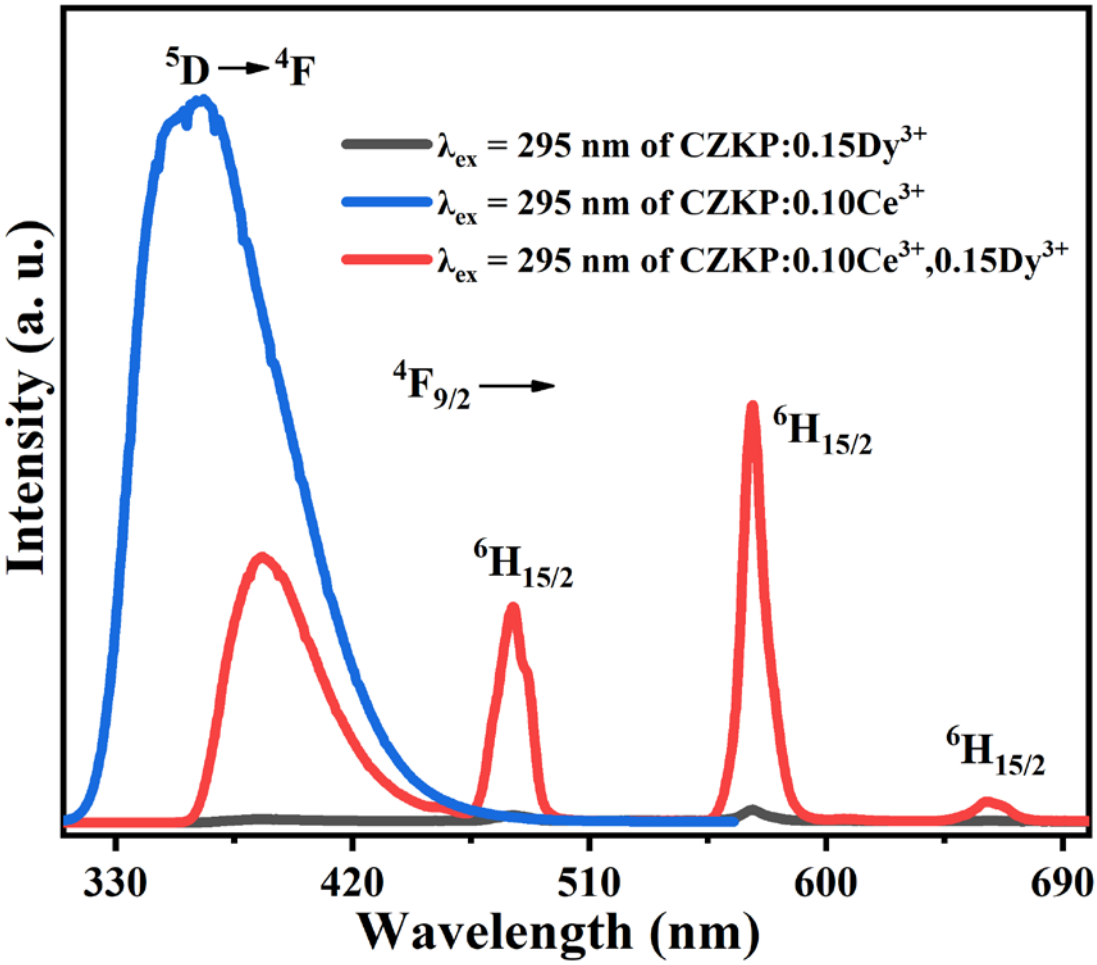

Fig. S9 PL curves of CZKP:0.15Dy^{3+}, CZKP:0.10Ce^{3+}, and CZKP: 0.10Ce^{3+},0.15Dy^{3+} under 295 nm excitation.

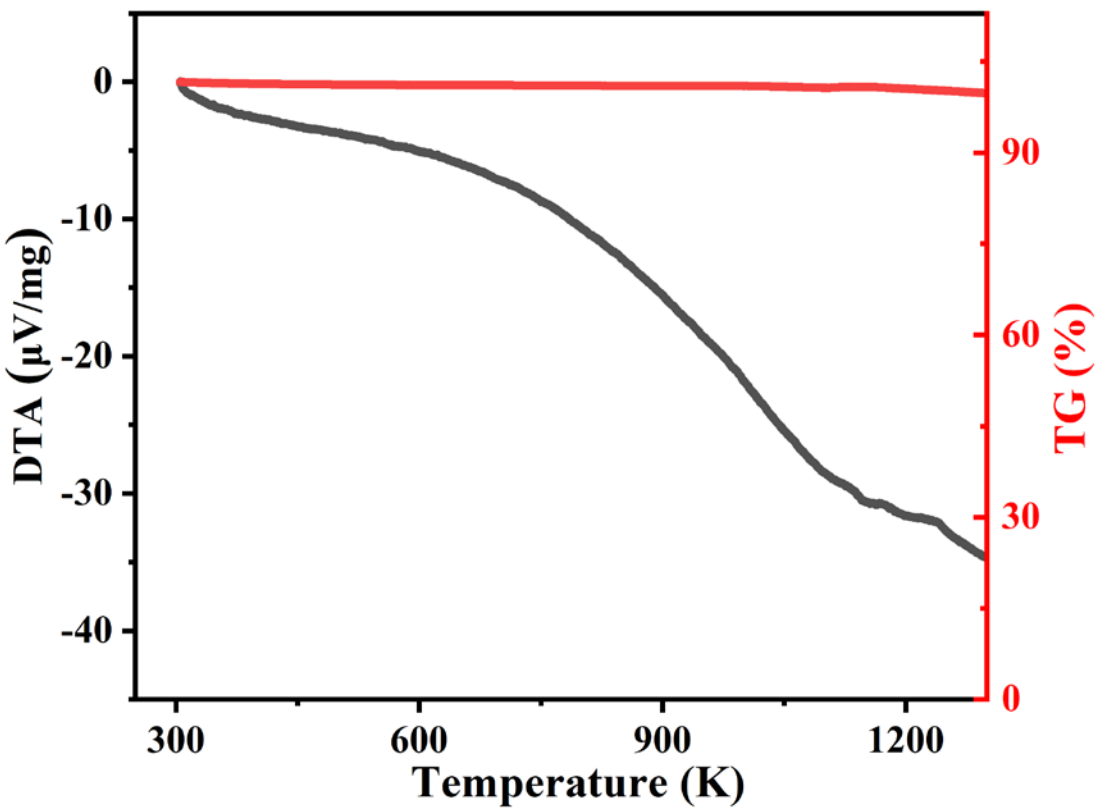

Fig. S10 TG-DTA curves of CZKP.

Table S1 Crystallographic data and refinement parameters for CZKP.

Compound	CZKP (JCPDS 50-0344)	CZKP (Our work)
Crystal system	Rhombohedral	Rhombohedral
Space group	*R*3c(161)	*R*3c(161)
Lattice parameters	$a = b = 10.4143$ Å $c = 37.125$ Å	$a = b = 10.4076$ Å $c = 37.0636$ Å
Unit cell volume	3487 $Å^3$	3476.798 $Å^3$
Cell angle	$\alpha = \beta = 90°$ $\gamma = 120°$	$\alpha = \beta = 90°$ $\gamma = 120°$
Z	6	6
R_p	-	9.94%
R_{wp}	-	13.60%
χ^2	-	4.35

Table S2 CIE coordinates and CCT of CZKP:0.10Ce^{3+},$y$$Dy^{3+}$($y$ = 0.05, 0.10, 0.15, 0.20, 0.25, and 0.30 mol) (λ_{ex} = 295 nm).

CZKP:0.10Ce^{3+},$y$$Dy^{3+}$	Coordinates (x, y)	CCT (K)
y = 0.05	(0.3220, 0.3281)	5540
y = 0.10	(0.3372, 0.3635)	4632
y = 0.15	(0.3431, 0.3759)	4387
y = 0.20	(0.3442, 0.3775)	4521
y = 0.25	(0.3418, 0.3721)	4526
y = 0.30	(0.3374, 0.3631)	4850

Bandgap determination

Based on diffuse reflectance, optical absorbance data can be obtained using the Kubelka – Munk transformation[1] as follows:

$$F(R) = (1 - R)^2/(2R) = K/S \quad \text{(S1)}$$

where R, K, and S stand for reflectance, absorption coefficient, and scattering coefficient, respectively.

The bandgap (E_g) is evaluated from the optical absorption near the absorption edge using Tauc relation[2]:

$$[F(R)h\nu]^{1/n} = A(h\nu - E_g) \quad \text{(S2)}$$

where hν and A correspond to the photon energy and proportionality constant, respectively. The n values of 1/2 and 2 correspond to direct and indirect allowed transitions, respectively. Owing to the fact that the indirect bandgap of the CZKP host is revealed by our computational energy band structure, the E_g value is determined using an extrapolation of the linear fitted region to $[F(R)h\nu]^{1/2} = 0$.

Ce^{3+} content-dependent photoluminescence for CZKP:Ce^{3+}

Fig. S6(a) shows the PLE and PL spectra of CZKP:$x$$Ce^{3+}$ (x = 0.05–0.25 mol). The PLE spectra monitored at 350 nm have a broad band with four splitting peaks at 243, 265, 295, and 310 nm, corresponding to the transitions from the ground state to the different crystal field splitting levels of the 5d state of Ce^{3+}.[3] The peak at 295 nm is the most prominent, and has been selected for the PL study. Upon the excitation at 295 nm, the CZKP:Ce^{3+} samples exhibit a broad emission band from 325 to 400 nm

with the peak at about 350 nm, originating from the 5d→4f transition of Ce^{3+} ion.[4] According to Figs. S6(b) and (c), the influences of dopant Ce^{3+} content on the 295 nm excitation and integral emission intensity keep a similar tendency. The optimal Ce^{3+} content is 0.10 mol.

Dy^{3+} content-dependent photoluminescence for CZKP:Dy^{3+}

Fig. S7(a) shows the PLE and PL spectra of CZKP:$y$$Dy^{3+}$ (y = 0.05–0.35 mol). Upon the monitoring wavelength at 575 nm, the main excitation peaks are attributed to the transitions from the ground state $^6H_{15/2}$ to the following excited states of Dy^{3+}: 295 ($^6F_{1/2}$), 325 ($^6P_{3/2}$), 350 ($^6P_{7/2}$), 365 ($^6P_{5/2}$), 388 ($^4I_{13/2}$), and 423 nm ($^4G_{11/2}$).[5] Upon the optimal excitation of 388 nm, the PL spectra show the three emissions located at 480 nm ($^6H_{15/2}$), 575 nm ($^6H_{13/2}$), and 660 nm ($^6H_{11/2}$).[5] The $^4F_{9/2}$→$^6H_{15/2}$ and $^4F_{9/2}$→$^6H_{13/2}$ emissions belong to the magnetic and electric dipole transitions (MDT and EDT), respectively. Generally, the EDT is more susceptible to the crystalline environment of dopant Dy^{3+} ion in comparison with the MDT. When Dy^{3+} occupies a low symmetry site, the EDT is dominant in the emission spectrum.[6] In this study, the EDT (yellow, 575 nm) is higher than the MDT (blue, 480 nm). Therefore, the dopant dysprosium occupies a low symmetry position in the CZKP host. According to Figs. S7(b) and (c), the influences of dopant Dy^{3+} content on the 388 nm excitation and integral emission intensity keep a similar tendency. The optimal Dy^{3+} content is 0.15 mol.

Content quenching mechanism for Ce^{3+}/Dy^{3+} single-doped CZKP

For the prepared Ce^{3+}/Dy^{3+} single-doped CZKP samples, the value of critical distance (R_c) is speculated based on Equation (3) proposed by Grabmaier and Blasse[7]:

$$R_c = 2(3V/4\pi\chi_c N)^{1/3} \quad \text{(S3)}$$

where V represents the volume per unit cell, χ_c means the critical content of doped ions, and N is the number of positions replaced per unit cell. In this case, V = 3476.798 $Å^3$, N = 18, χ_c = 0.10 mol for Ce^{3+}, and χ_c = 0.15 mol for Dy^{3+}. The non-radiative energy transfer process can be classified into two types: exchange interaction and multipole–multipole interaction. The exchange interaction dominates when the R_c value is less than 5 Å, otherwise the multipolar interaction prevails. The R_c values for the Ce^{3+}/Dy^{3+} single-doped CZKP samples are 15.45/13.50 Å, respectively.

The concrete multipolar interaction is analyzed according to the Van Uitert model as follows[8]:

$$I/\chi = K[1 + \beta(\chi)]^{\theta/3^{-1}} \quad \text{(S4)}$$

where β and K stand for constants. The correlation between emission intensity (I) and doping ions concentration (χ) is illustrated in Equation (S4). The values of θ are 6, 8, and 10, corresponding to electric dipole–dipole, dipole–quadrupole and quadrupole–quadrupole interactions, respectively. The value of $\beta(\chi)^{\theta/3}$ is far larger than 1. Hence, the simplified expression of Equation (S4) is illustrated as follows:

$$\log(I/\chi) = A - (\theta/3)\log(\chi) \quad \text{(S5)}$$

where A is a constant, which can be determined for the CZKP matrix. Thus, based on

Equation (S5), we can speculate the value of θ from the slope $(-\theta/3)$.

Fig. S8 shows the relationship of log(I/χ) versus log(χ) in the Ce^{3+}/Dy^{3+} single-doped CZKP samples. The fitted linear slopes ($-\theta/3$) of −1.764 for Ce^{3+} and −1.588 for Dy^{3+} correspond to θ = 5.292 for Ce^{3+} and θ = 4.764 for Dy^{3+}, respectively. Hence, the dipole–dipole interaction is dominant for the content quenching of the Ce^{3+}/Dy^{3+} single-doped CZKP samples.

Decay time

The optical decay time is fitted via the second-order exponential function with the following equation[9]:

$$I(t) = I_0 + A_1 \exp(-t/\tau_1) + A_2 \exp(-t/\tau_2) \quad \text{(S6)}$$

where t represents the time, I(t) is the emission intensity corresponding to time t, I_0 is the initial emission intensity corresponding to time t = 0, A_1 and A_2 are constants, and τ_1 and τ_2 are lifetimes for the exponential components. The average lifetime τ_{ave} can be obtained by the formula as follows:

$$\tau_{ave} = (A_1\tau_1^2 + A_2\tau_2^2)/(A_1\tau_1 + A_2\tau_2) \quad \text{(S7)}$$

Energy transfer mechanism

Based on the Dexter's energy transfer theory of multipolar interaction and Reisfeld's approximation, the following formula is given[10]:

$$\frac{\tau_0}{\tau} \propto C^{n/3} \quad \text{(S8)}$$

where τ_0 is the lifetime of Ce^{3+}, and τ is the lifetime of Ce^{3+} in the presence of Dy^{3+}. *C*

stands for the total content of Ce^{3+} and Dy^{3+}. The value of n = 6, 8, and 10 corresponds to dipole–dipole, dipole–quadrupole and quadrupole–quadrupole interactions, respectively.

Thermal quenching mechanism

To investigate the thermal quenching mechanism of the CZKP:Ce^{3+},Dy^{3+} samples, the activation energy (E_a) was calculated via the following Arrhenius equation:

$$\ln[(I_0/I(T)) - 1] = \ln A - (E_a/KT) \quad \text{(S9)}$$

where I_0 is the initial emission intensity of the phosphor at room temperature, I(T) is the emission intensity at testing temperature T, A is an invariable constant for a certain host, and K represents the Boltzmann constant (8.629×10^{-5} eV/K). Based on the equation, the relationship between $\ln[(I_0/I(T)) - 1]$ versus 1/kT was shown.

Color stability

The color stability can be quantifiably described by the chromaticity shift (ΔE) using the following equation[11]:

$$\Delta E = \sqrt{(u_f' - u_i')^2 + (v_f' - v_i')^2 + (w_f' - w_i')^2} \quad \text{(S10)}$$

where $u' = 4x/(3 - 2x + 12y)$, $v' = 9y/(3 - 2x + 12y)$, and $w' = 1 - u' - v'$. u' and v' are the chromaticity coordinates in the $u'v'$ uniform color space. x and y are the chromaticity coordinates in the CIE1931 color space. i and f represent room temperature and working temperature, respectively.

Calculation on CCT

The parameter of correlated color temperature (CCT) can be speculated using McCany empirical formula, which is illustrated as:

$$\mathrm{CCT} = -449\mathrm{n}^3 + 3525\mathrm{n}^2 - 6823.3\mathrm{n} + 5520.33 \quad \text{(S11)}$$

where n equals (x – 0.3320)/(y – 0.1858).

References

1 P. Kubelka and F.Z. Munk, *Z. Tech. Phys.*, 1931, **12**, 593–601.

2 J. Tauc, A. Menth and D.L. Wood, *Phys. Rev. Lett.*, 1970, **25**, 749–752.

3 R. L. Kohale and S. J. Dhoble, *J. Mol. Struct.*, 2018, **1170**, 18–23.

4 K. Dev, A. Selot, G. B. Nair, V. L. Barai, H. Z. Haque, M. Aynyas and S. J. Dhoble, *J. Lumin.*, 2019, **206**, 380–385.

5 S. Y. Xin, M. Gao, J. L. Ma, H. Dai and G. Zhu, *Dalton Trans.*, 2020, **49**, 15800–15809.

6 J. Zhu, J. Y. Xiang, Y. K. Zheng, D. Yang, Z. Y. Fang and Y. Mao, *J. Alloys Compd.*, 2020, **831**, 154809.

7 G. Blasse, *Phys. Lett. A*, 1968, **28**, 444–445.

8 L.G. Van Uitert, *J. Electrochem. Soc.*, 1967, **114**, 1048–1053.

9 H. F. Li, Y. L. Jia, T. F. Ma, R. Pang, W. Z. Sun, D. Li, C. Y. Li, J. P. Fu, S. Zhang and L. H. Jiang, *Eur. J. Inorg. Chem.* 2016, **6**, 867–873.

10 B. Chen, A. S. Susha, C. J. Reckmeier, S. V. Kershaw, Y. Wang, B. Zou, H. Z. Zhong and A.L. Rogach, *Adv. Mater.*, 2017, **29**,1604284.

11 J. Liang, B. Devakumar, L. L. Sun, S. Y. Wang, Q. Sun and X. Y. Huang, *J. Mater. Chem. C*, 2020, **8**, 4934-4943.